

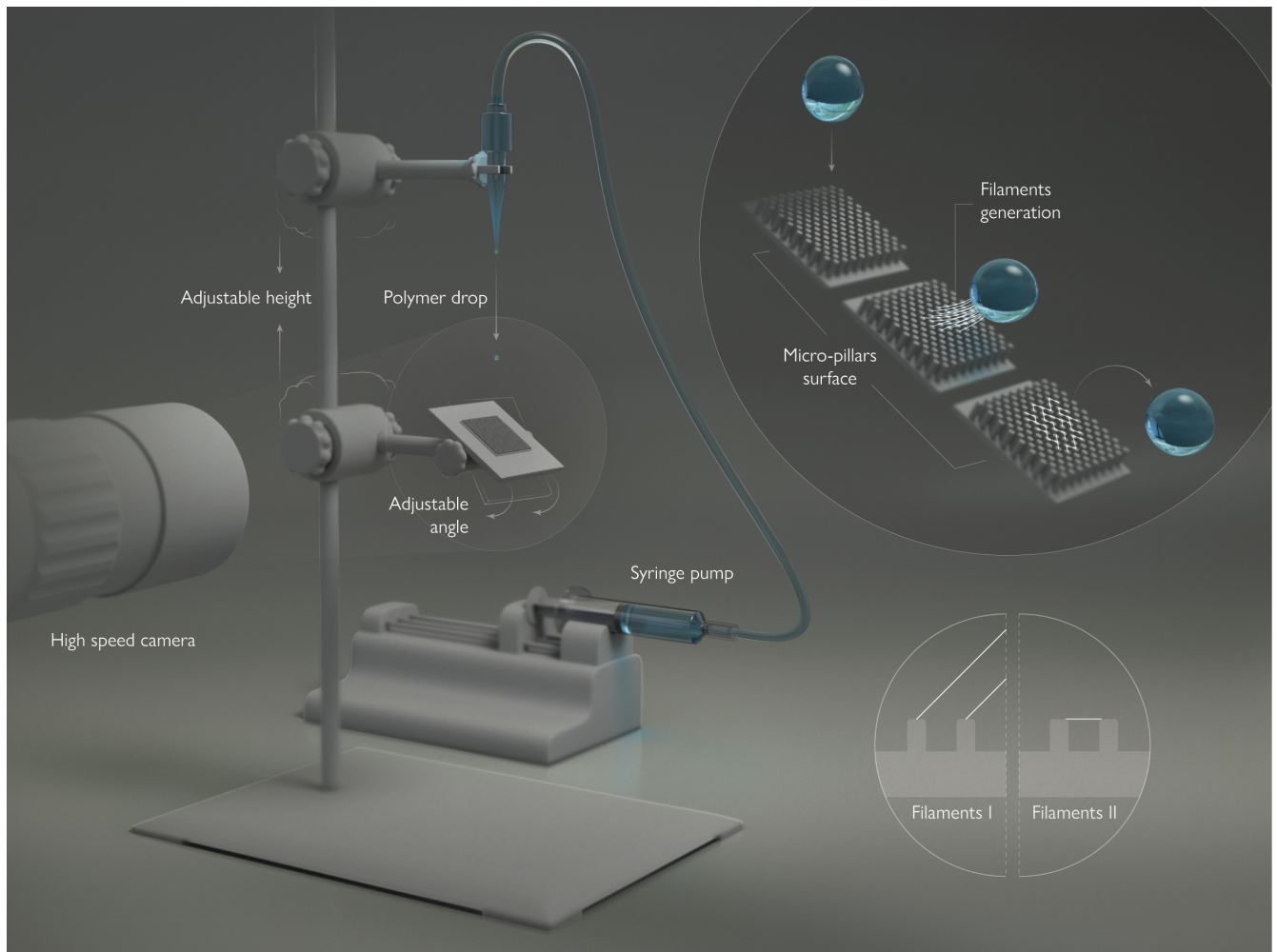
Supplementary Material for  
Direct imaging of polymer filaments pulled from rebounding drops

Zi Qiang Yang,<sup>1</sup> Peng Zhang,<sup>2</sup> Meng Shi,<sup>1</sup> Ali Al Julaih,<sup>1</sup> Himanshu Mishra,<sup>2</sup> Enzo Di Fabrizio,<sup>3</sup> and Sigurdur T. Thoroddsen<sup>\*1</sup>

<sup>1</sup>*Division of Physical Sciences and Engineering, King Abdullah University of Science and Technology (KAUST), Thuwal 23955-6900, Saudi Arabia*

<sup>2</sup>*Division of Biological and Environmental Science and Engineering, King Abdullah University of Science and Technology (KAUST), Thuwal 23955-6900, Saudi Arabia*

<sup>3</sup>*Department of Applied Science and Technology, Politecnico di Torino, Torino 10129, Italy*



Supplementary Fig. 1. Schematic drawing of the experimental set-up, with high-speed video camera viewing the dynamics of a polymer droplet impacting on a super-hydrophobic substrate with various inclination angle  $\theta$ . The high-speed video camera captures the impact dynamics of polymer droplet in the side-view. In some experiments a second camera views this in a direction perpendicular to the inclined super-hydrophobic substrate. The inset on the top right, shows a zoomed in view of a polymer droplet impacting on the super-hydrophobic micro-pillars with polymer filaments pulled out of the drop free surface during the rebounding. These filaments attach to adjacent micro-pillars (see bottom inset) which allows their further study using electron microscopy. Illustration created by Ivan Gromicho. Scientific Illustrator at Research Communication and Publication Services. Office of the Vice President for Research - King Abdullah University of Science and Technology.

Substrates	Equilibrium contact angle (°)	Nature of the substrate	Sq (nm)	Sz (nm)	Sa (nm)
Cylindrical Pillars	0	Superhydrophilic	—	—	—
Flat mica sheet	$2.4 \pm 0.3$	Superhydrophilic	0.071	0.651	0.056
Silica treated with plasma	$17.4 \pm 0.7$	Hydrophilic	0.280	15.679	0.201
Flat silica	$36.5 \pm 1.2$	Hydrophilic	0.737	35.805	0.570
Silica coated with FDTs	$98 \pm 1.6$	Hydrophobic	0.304	31.449	0.190
Cylindrical Pillars coated with FDTs	$140 \pm 2$	Hydrophobic	—	—	—
One time Glaco-coated surface	$152 \pm 1.5$	Superhydrophobic	140.556	952.908	113.957
Four time Glaco-coated surface	$162 \pm 3$	Superhydrophobic	170.643	1258.250	126.217

Supplemental Table I. Characterization of various surfaces investigated in this work. contact angle, contact angle hysteresis, surface mean roughness,  $S_a$ , maximum height,  $S_z$  and rms roughness,  $S_q$ , for all tested surfaces.

$c$	10 ppm	50 ppm	100 ppm	200 ppm	400 ppm	1000 ppm
$c/c^*$	0.02	0.09	0.18	0.35	0.71	1.76
Weight concentration, $w$ , [g/L]	0.01	0.05	0.10	0.20	0.40	1.00
Density, $\rho$ [g/cm <sup>3</sup> ]	0.996	0.996	0.996	0.996	0.996	0.996
Viscosity, $\mu$ [mPa.s]	0.976	1.03	1.08	1.18	1.20	1.23
Surface tension, $\sigma$ [mN/m]	73.1	68.3	68.2	62.2	62	62

Supplemental Table II. Liquid properties of dilute PEO solutions for molecular weight  $4 \times 10^6$  g/mol and water drop (the critical overlap concentration  $c^* \approx 567$  ppm [1])

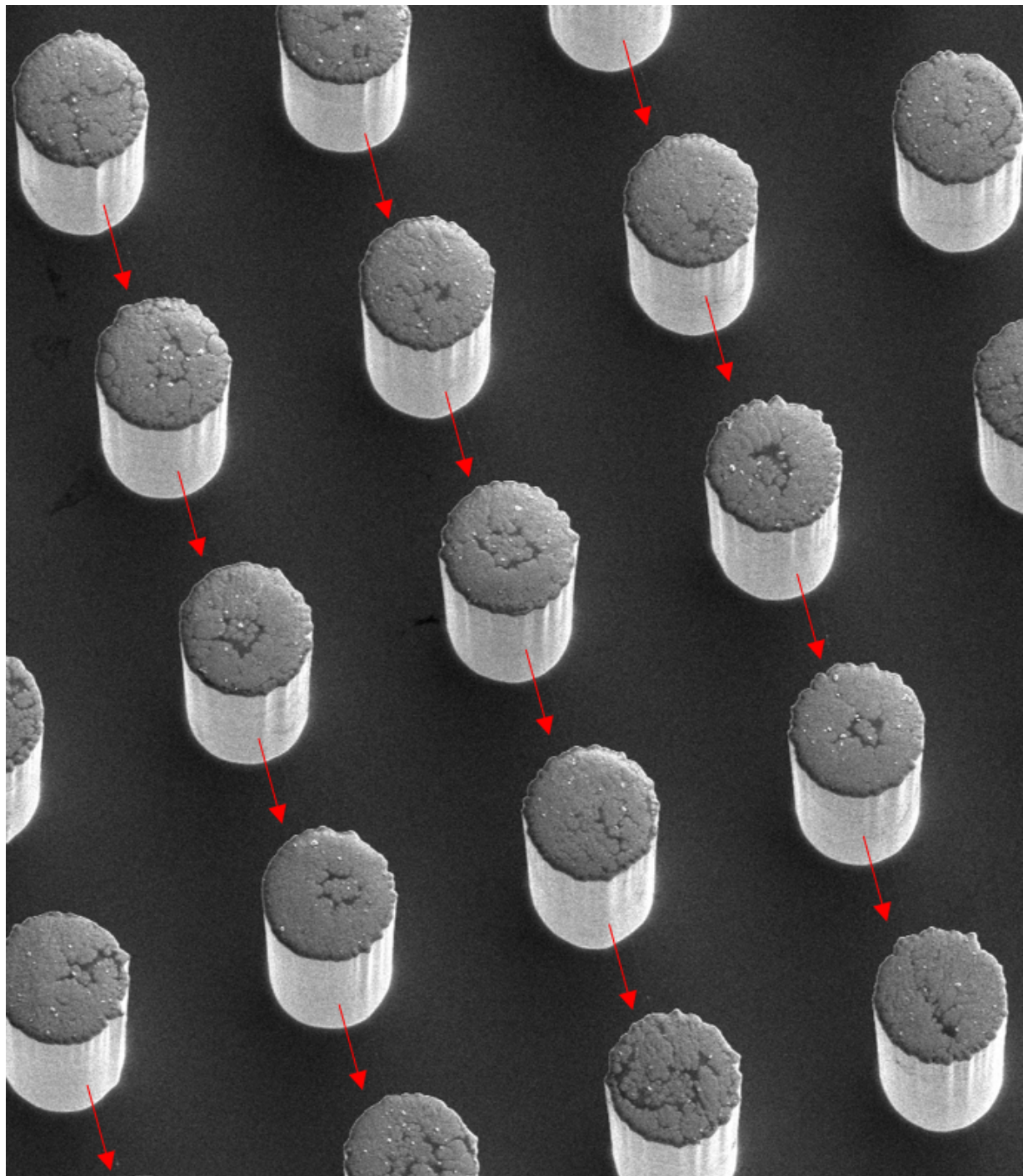
## S1. EXPERIMENTAL SETUP AND LIQUID PROPERTIES

The experimental set-up used for drop impacts on inclined micro-pillared substrates, to collect PEO and DNA filament bundles, is sketched in Supplementary Fig. S1. Table S.I gives the wetting properties of the various substrates in terms of the equilibrium contact angles. Table S.II lists the effect of PEO polymer concentration in the water drop, on the liquid properties of density, viscosity and surface tension.

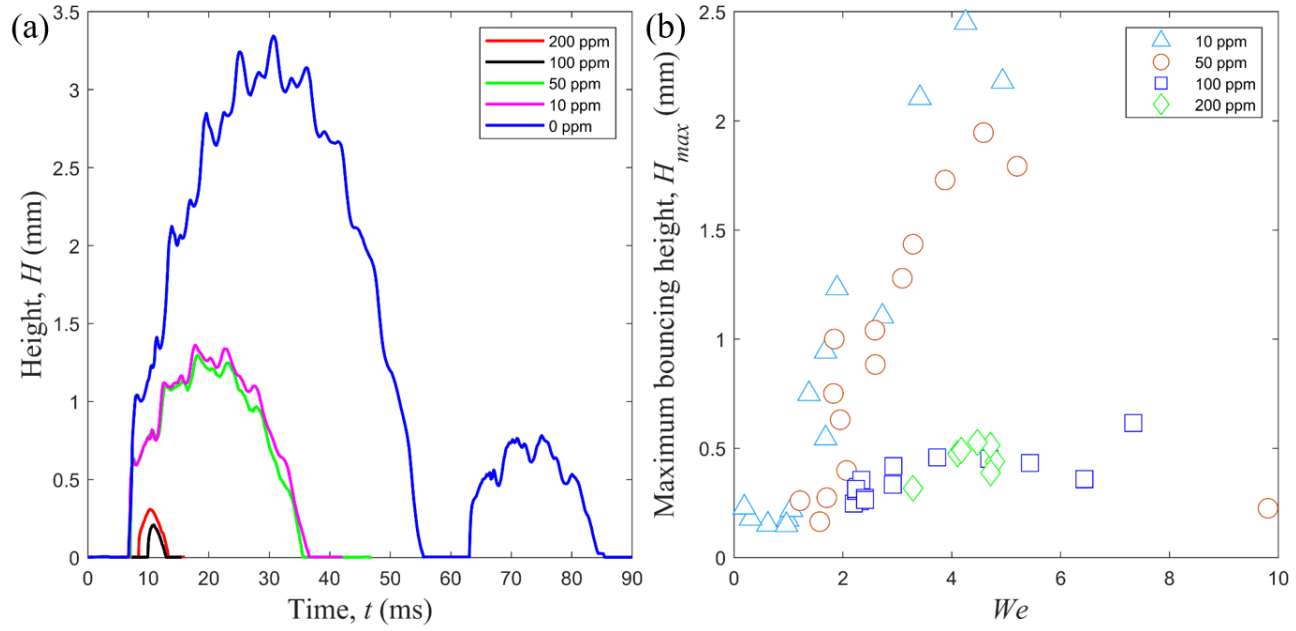
## S2. POLYMER DEPOSITION AND BOUNCING HEIGHTS

After the drop rebounds from pillared surface the deposited PEO or DNA bundles can be imaged by scanning electron microscopy (SEM). These bundles are homogeneously suspended and distributed between the edge of adjacent micro-pillars as shown in Supplemental Fig. S2. The filaments are aligned between the pillars in the direction of the rebounding of the drop.

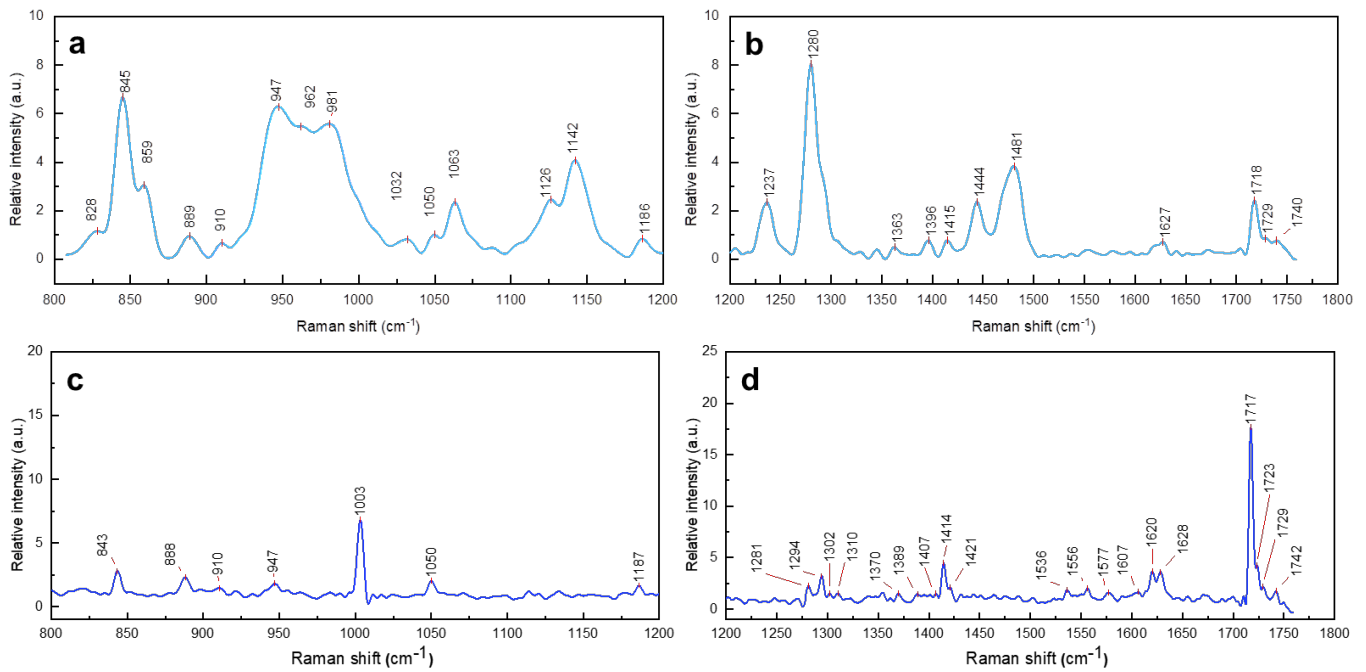
Figure S3 shows how the concentration of the PEO polymer reduces the rebounding height of the drops. In Fig. S3(a) the trajectory of the bottom of the drop is shown as a function of time from first contact with the substrate. In Fig. S3(b) the maximum bouncing height is shown over a range of impact Weber number and different PEO concentrations.



Supplementary Fig. 2. Regular DNA filaments between numerous pillars. The red arrows are next to the very faint filaments and point in the direction of the rebounding of the drop. For scale the pillar centers are spaced by  $50 \mu\text{m}$ .



Supplementary Fig. 3. (a) Bouncing trajectories with different PEO concentrations for drop impacts on cylindrical micro-pillars coated with FDTTS, under the same impact conditions  $D \approx 1.4 \pm 0.2$  mm,  $U \approx 0.45 \pm 0.02$  m/s. The symbols correspond to different PEO concentrations: 200 ppm —; 100 ppm —; 50 ppm —; 10 ppm —; 0 ppm —. (b) Maximum bouncing height with increasing Weber number values for different PEO concentration.



Supplementary Fig. 4. Raman spectral peaks of PEO in bulk (a, b) and PEO nano-filament suspended between micro-pillars after the drop impact (c, d).

### S3. MOLECULAR STRUCTURE CHARACTERIZATION OF PEO AND DNA NANO-FILAMENTS WITH RAMAN SPECTROSCOPY

#### A. Raman analysis of PEO nano-filaments

To understand the molecular structures of the drop-impact-deposited PEO nano-filaments, we characterized its Raman spectra and compared with the PEO in bulk. First, the Raman spectra of PEO in bulk (Supplemental Fig. 4a) is essentially the same as previously reported [2–4]. Briefly, these peaks between  $800\text{ cm}^{-1}$  and  $1150\text{ cm}^{-1}$  denote the C–O stretching in PEO skeletal and  $\text{CH}_2$  rocking vibration modes. The specific peaks indicate the mixtures of various conformations [4]. Peaks at  $828\text{ cm}^{-1}$ ,  $845\text{ cm}^{-1}$ , and  $859\text{ cm}^{-1}$  can be assigned to the  $xGx-xTx$  ( $G$ : gauche;  $T$ : trans) conformation, while the peaks at  $947\text{ cm}^{-1}$ ,  $962\text{ cm}^{-1}$ ,  $981\text{ cm}^{-1}$  (Supplemental Fig. 4a) can be signed to  $xGT-TGx$  and  $xTT-(GTx)$  conformation [5]. Peaks at  $1237\text{ cm}^{-1}$  and  $1280\text{ cm}^{-1}$  are related to the  $\text{CH}_2$  antisymmetric twisting vibration with respect to the C–C axis.

Peaks between  $1320\text{ cm}^{-1}$  and  $1420\text{ cm}^{-1}$  (Supplemental Fig. 4b) correspond to the  $\text{CH}_2$  wagging vibration. The peaks between  $1450\text{ cm}^{-1}$  and  $1500\text{ cm}^{-1}$  (Supplemental Fig. 4b) correspond to the  $\text{CH}_2$  bending vibration of the PEO chain, and the main peak is located at  $1481\text{ cm}^{-1}$  indicates the molecules are in semi-solid (semi-dry) condition, which is in accord with our experimental condition, as mentioned in previous section. The peaks at  $1627\text{ cm}^{-1}$  and  $1718\text{ cm}^{-1}$  (Supplemental Fig. 4b) normally can be signed to C=O vibration, while it should not be present in PEO. We think this C=O group most probably indicating that the PEO molecules oxidized in air [6, 7].

Compared to the PEO in bulk, the Raman spectra of suspended PEO nano-filaments (Supplemental Fig. 4c and d) have several important differences:

**I: Ultra-high spectra resolution due to self-deconvolution in single-molecule level.** The Raman band of PEO nano-filaments are significantly sharper and has a ultra-high resolution compare to those of PEO in bulk. For example, the C=O stretching peak at  $1627\text{ cm}^{-1}$  is wider in the PEO bulk sample, while in PEO nano-filaments, apart from the peak at  $1628\text{ cm}^{-1}$  (we consider it to be the C=O stretching signal with a slight shifting from  $1627\text{ cm}^{-1}$ ) two new peaks can be separated and recognized at  $1607\text{ cm}^{-1}$ ,  $1620\text{ cm}^{-1}$ . These two peaks are most probably from the additive inhibitor, butylated hydroxytoluene (BHT) [8]. Meanwhile, the BHT Raman signal at  $1050\text{ cm}^{-1}$  is much sharper and cleaner than the one under PEO bulk condition. Since this BHT has a low concentration (200-

500 ppm) in this PEO product, its signal can easily be hidden in background, i.e., the PEO signal. However, taking advantage of this PEO nano-filaments preparation, we can recognize the BHT Raman signal without any extra sample pre-treatment process. We think this ultra-high spectral resolution is a result of ultra-small sample amount induced self-deconvolution effect. The Raman spectra from PEO bulk is the average of a large number of PEO molecules, which causes significant broadening and overlapping of the Raman peaks. It limits the spectral resolution and relies heavily on deconvolution during the data analysis [9]. On the contrary, based on a typical molecular structure model of PEO (72 helical model, seven repeat units in the trans-gauche-trans (TGT) conformation of sequences -O-CH<sub>2</sub>-CH<sub>2</sub>-O- on two turns in an identity period) [3], the diameter of the each PEO helical chain is about 3 Å [2]. Therefore, in the PEO nano-filament which is in the 10-nm thickness range, only around 30 PEO polymer chains assemble together. Hence, the molecular averaging effect is suppressed significantly, which produced very sharp Raman signal and remarkably enhance the spectral resolution.

**II: Conformation confinement and of PEO nano-filaments.** As we mentioned in the previous section, the peaks between 800 cm<sup>-1</sup> and 1300 cm<sup>-1</sup> are mainly related to the PEO chain conformation. Unlike the wide and complex peaks of PEO in bulk condition, which have various molecular conformations, the PEO nano-filaments have a very clean and sharp Raman peaks. For example, the two triplet peaks at around 845 cm<sup>-1</sup> and around 962 cm<sup>-1</sup> of bulk PEO sample unified to two singlet peaks at 843 cm<sup>-1</sup> and 947 cm<sup>-1</sup>, indicating that the molecular conformation in PEO nano-filaments are much more homogeneous. And the peak at 843 cm<sup>-1</sup> resolves that the PEO molecules in the nano-filaments are mainly in helical conformation, which is highly ordered and normally found in crystalline solid state PEO [4, 5]. We think that during the PEO droplet bouncing, the stretching force will apply on the nano-filaments and will confine the PEO molecule chain in a relative uniform way. The peak at 888 cm<sup>-1</sup> indicates another main components as the *xGx-xTx* conformation [4]. Meanwhile, the Raman signal between 1100 cm<sup>-1</sup> and 1150 cm<sup>-1</sup>, 1450 cm<sup>-1</sup> and 1500 cm<sup>-1</sup> in PEO nano-filaments are very weak compare with the PEO in bulk. Since these areas mainly related to the CH<sub>2</sub> vibration modes (wagging, rocking, and bending), these weak Raman signals indicate that these CH<sub>2</sub> vibration modes were suppressed, perhaps this is the results of molecular confinement in the PEO nano-filaments.

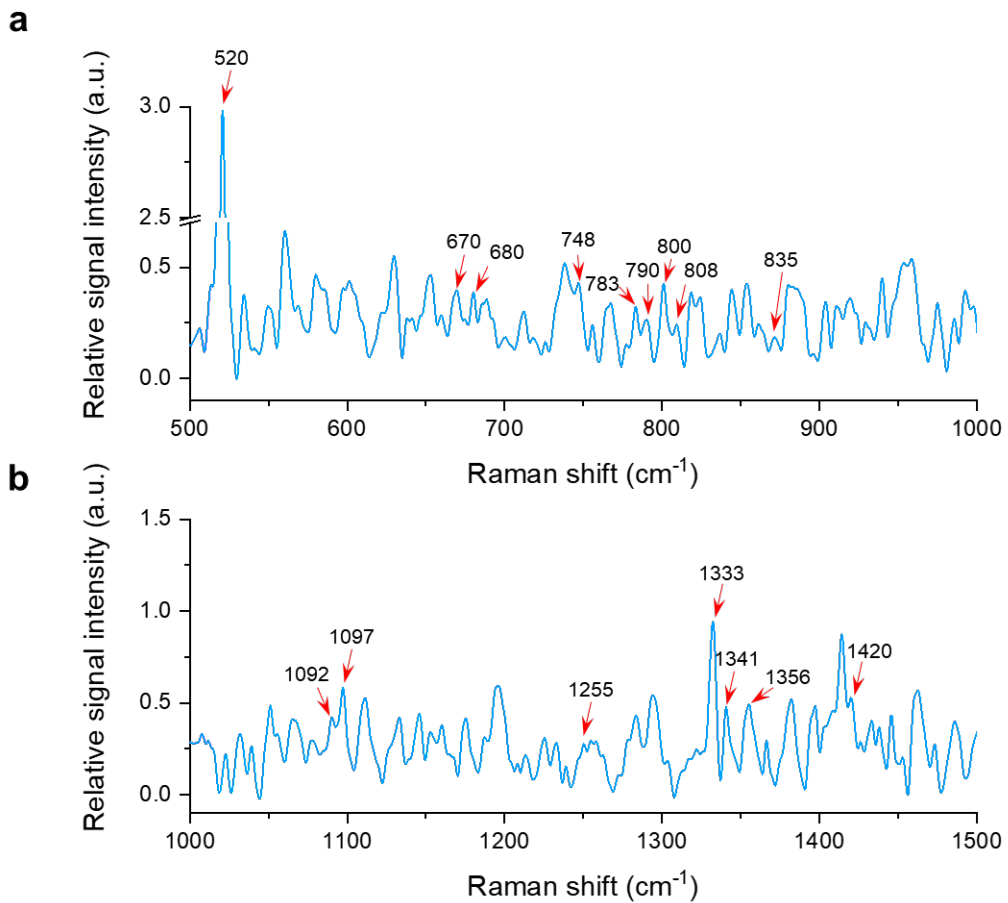
**III: Accelerated oxidation of PEO nano-filaments.** Although PEO can easily be oxidized in ambient air [6], the additive antioxidant such as BHT can provide a good protection for it. Therefore, only a small peak of C=O at 1718 cm<sup>-1</sup> was observed under bulk PEO condition (Supplemental Fig. 4b). However, the Raman peak of C=O at 1717 cm<sup>-1</sup> in PEO nano-filaments is significantly enhanced (Supplemental Fig. 4d), which indicates the oxidized PEO ratio in nano-filaments are much higher than in the bulk. We think this is mainly because of the small thickness scale of the nano-filaments, making the PEO molecules have a much higher probability of reacting with the oxygen in the air and producing large number of C=O groups.

## B. Raman analysis of DNA nano-filaments

DNA is a unique molecule made of four types of nucleotides, which are connected covalently into a polynucleotide chain with a sugar-phosphate backbone, from which the bases (Adenine (A), Guanine (G), Thymine (T), and Cytosine (C)) extend. A DNA molecule is composed of two DNA strands held together by hydrogen bonds between the paired bases and twisted into a double-helix. Currently, the molecular structure analysis of DNA is mainly performed along two streams: DNA sequencing and DNA conformation analysis. Since we are using a commercial  $\lambda$ -DNA molecules which contain 485027 bp with a known sequence, the Raman analysis will be focused on its conformation in the nano-filaments. There are three different conformation of DNA, A-form, B-form, and Z-form [10]. Among them, the B-form DNA is known to be the ideal DNA structure, while the A-form and Z-form DNA can be present locally according to the environmental stresses, such as hydration [11, 12] and an ionic environment [13]. Furthermore, according to our previous study, the hydrodynamic force can be another factor inducing bio-molecules conformation change [14]. Herein, we used Raman spectroscopy to characterize the DNA molecular conformation in the nano-filaments.

The peaks at 670 cm<sup>-1</sup>, 680 cm<sup>-1</sup>, and 1333 cm<sup>-1</sup> are assigned to G-base. Peak at 1341 cm<sup>-1</sup> is assigned to A-base. Peaks at 784 cm<sup>-1</sup> and 1255 cm<sup>-1</sup> are assigned to C-base, while peaks at 748 cm<sup>-1</sup>, 790 cm<sup>-1</sup>, and 1356 cm<sup>-1</sup> are indicating T-base. Meanwhile, the peaks at 800 cm<sup>-1</sup>, 808 cm<sup>-1</sup>, 1092 cm<sup>-1</sup>, 1097 cm<sup>-1</sup>, and 1420 cm<sup>-1</sup> indicating the chemical-bond vibrations of O-P-O and H-C-H in the backbone of the DNA. The peaks at 680 cm<sup>-1</sup>, 800 cm<sup>-1</sup>, 835 cm<sup>-1</sup> and 1333 cm<sup>-1</sup> indicating that the DNA molecules in nano-filaments are mainly in B-form, and small portion of the molecules are conformed as A-form (peaks at 670 cm<sup>-1</sup> and 808 cm<sup>-1</sup>) [15, 16]. According to previous reports, the A-form is supposed to be the dominant conformation of DNA at humidity lower than 75% [17]. However, in our experiment we observe that the B-form DNA is the favorite conformation in nano-filaments at ~ 45% humidity.

We think that during the drop bouncing, the DNA molecules are stretched by the hydrodynamic forces, which is



Supplementary Fig. 5. Raman spectra of DNA nano-filaments deposited between micro-pillars by rebounding drops after impact on an inclined substrate, in the range of 500-1000 cm<sup>-1</sup> (a) and 1000-1500 cm<sup>-1</sup> (b). The peak at 520 cm<sup>-1</sup> indicates signal from the Si substrate.

equivalent to previous report of stretching of the DNA in solution by surface tension of water during the liquid bridge jumping between micro-pillars during drop evaporation [14, 18]. However, during the impact bouncing the stretching is stronger providing more strain and thinner filaments. Meanwhile, since the transformation from B-form to A-form is mainly induced by dehydration at relatively low humidity, we think the residual stress in DNA nano-filaments provides a force to compete with the contractive force during dehydration and thereby preventing the B-to-A transformation in the nano-filaments. Furthermore, the peak at 835 cm<sup>-1</sup> denotes that the base ratio (AT:CG) in this DNA molecule is 50:50, which is in accord with the  $\lambda$ -DNA information which we used.

- 
- [1] Pack, M. Y., Yang, A., Perazzo, A., Qin, B. & Stone, H. A. Role of extensional rheology on droplet bouncing. *Phys. Rev. Fluids* **4**, 123603 (2019).
- [2] Yoshihara, T., Tadokoro, H. & Murahashi, S. Normal vibrations of the polymer molecules of helical conformation. iv. polyethylene oxide and polyethylene-d 4 oxide. *J. Chem. Phys.* **41**, 2902–2911 (1964).
- [3] Sagitova, E. *et al.* Raman analysis of polyethylene glycols and polyethylene oxides. In *J. Phys. Conf. Ser.*, vol. 999, 012002 (IOP Publishing, 2018).
- [4] Matsuura, H. & Fukuhara, K. Vibrational spectroscopic studies of conformation of poly (oxyethylene). ii. conformation-spectrum correlations. *J. Polym. Sci. B Polym. Phys.* **24**, 1383–1400 (1986).
- [5] Samuel, A. Z. & Umapathy, S. Energy funneling and macromolecular conformational dynamics: a 2d raman correlation study of peg melting. *Polym. J.* **46**, 330–336 (2014).
- [6] Harding, J. R., Amanchukwu, C. V., Hammond, P. T. & Shao-Horn, Y. Instability of poly (ethylene oxide) upon oxidation

- in lithium-air batteries. *J. Phys. Chem.* **119**, 6947–6955 (2015).
- [7] de Sainte Claire, P. Degradation of peo in the solid state: A theoretical kinetic model. *Macromolecules* **42**, 3469–3482 (2009).
- [8] Babu, P. C., Sundaraganesan, N., Dereli, Ö. & Türkkan, E. Ft-ir, ft-raman spectra, density functional computations of the vibrational spectra and molecular geometry of butylated hydroxy toluene. *Spectrochim Acta A Mol Biomol Spectrosc* **79**, 562–569 (2011).
- [9] Thomas Jr, G. J. & Agard, D. A. Quantitative analysis of nucleic acids, proteins, and viruses by raman band deconvolution. *Biophys. J.* **46**, 763–768 (1984).
- [10] Marini, M. *et al.* DNA studies: Latest spectroscopic and structural approaches. *Micromachines* **12**, 1094 (2021).
- [11] Franklin, R. E. & Gosling, R. G. Molecular configuration in sodium thymonucleate. *Nature* **171**, 740–741 (1953).
- [12] de Rosa, M., Zacarias, S. & Athanasiadis, A. Structural basis for z-DNA binding and stabilization by the zebrafish z-DNA dependent protein kinase pkz. *Nucleic Acids Res.* **41**, 9924–9933 (2013).
- [13] Watson, J. D. & Crick, F. H. Molecular structure of nucleic acids: a structure for deoxyribose nucleic acid. *Nature* **171**, 737–738 (1953).
- [14] Zhang, P. *et al.* A droplet reactor on a super-hydrophobic surface allows control and characterization of amyloid fibril growth. *Commun. Biol.* **3**, 1–13 (2020).
- [15] Thomas Jr, G. J. Raman spectroscopy of protein and nucleic acid assemblies. *Annu. rev. biophys. biomol. struct.* **28**, 1–27 (1999).
- [16] Coluccio, M. *et al.* From nucleotides to DNA analysis by a sers substrate of a self similar chain of silver nanospheres. *J Opt.* **17**, 114021 (2015).
- [17] Wilkins, M. H. F., Stokes, A. R. & Wilson, H. R. Molecular structure of nucleic acids: molecular structure of deoxypentose nucleic acids. *Nature* **171**, 738–740 (1953).
- [18] Bensimon, A. *et al.* Alignment and sensitive detection of DNA by a moving interface. *Science* **265**, 2096–2098 (1994).